CyberSAR

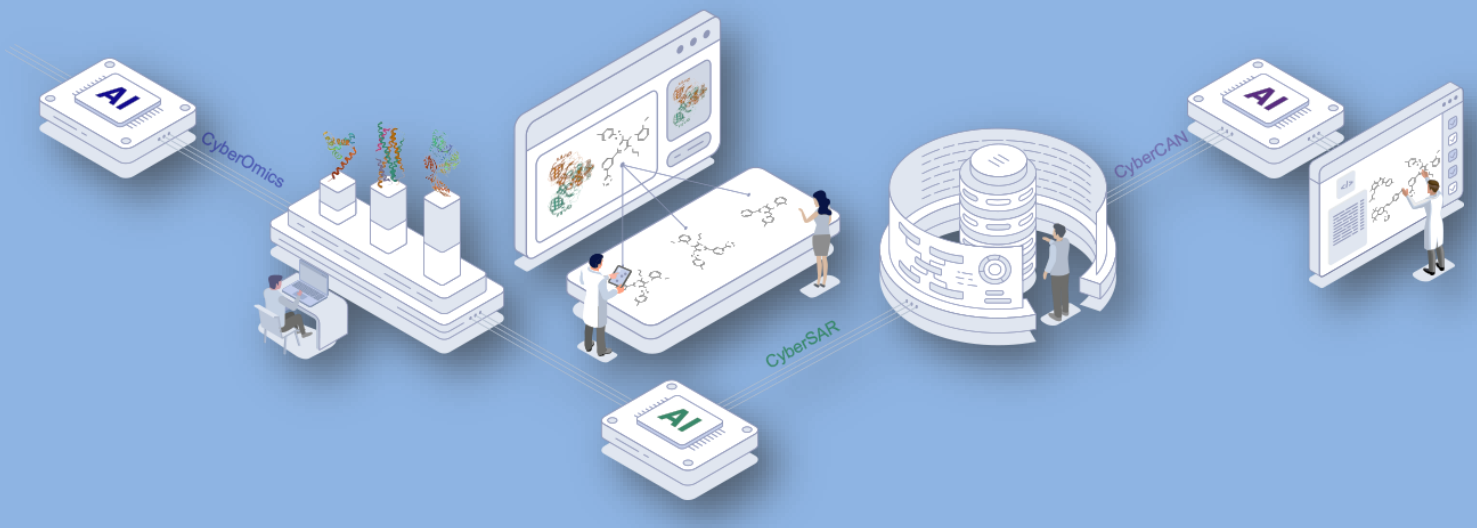

Molecular design and optimization process of BMS-986172, an MGAT2 inhibitor developed by BMS

FEBRUARY 2024

Cyber analyzed the molecular design and optimization process of BMS-986172, an MGAT2 inhibitor developed by BMS

Part I

MGAT2 has become a potential therapeutic target for metabolic diseases in recent years, BMS has developed a potent and highly selective MGAT2 inhibitor BMS-963272 (compound 1), as the first clinical candidate of BMS, and has been evaluated in phase I clinical trials, compound 1 can increase plasma long-chain dicarboxylic acids, show a strong pharmacodynamic biomarker modulation effect, increase glucagon GLP-1 and PYY, and reduce the weight of subjects. However, **BMS-963272 was discontinued from clinical trials due to glucuronidation of tetrazolium and isomerization of C-C double bonds in the parent nucleus of dihydropyrrolidone**. BMS identified compound 12 (**BMS-986172**) as a second clinical candidate through a series of screenings, which can provide valuable experience for structural optimization of similar projects.

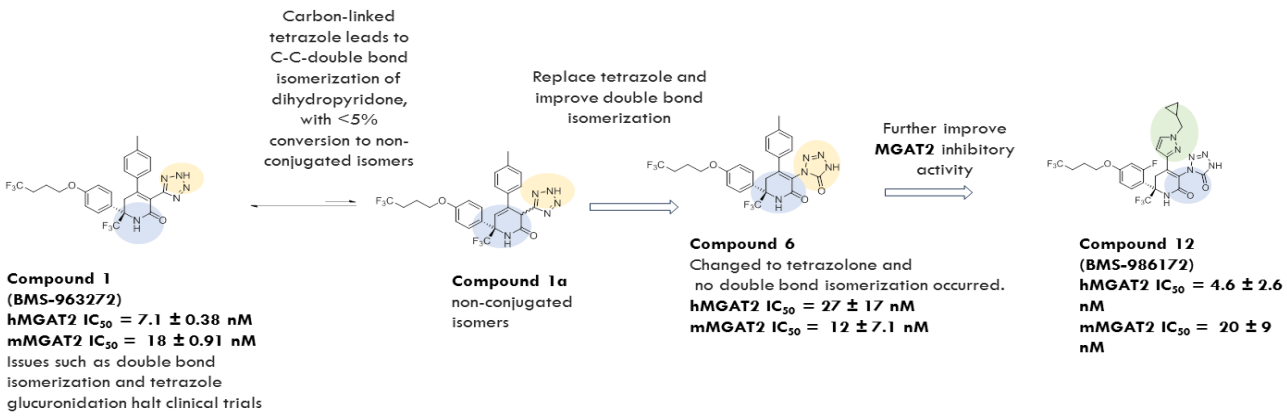

Part II

Monoacylglycerol (MAG) is absorbed in the small intestine, converted into triglycerides (TAGs) in intestinal cells, and eventually secreted into chylomicrons for distribution in the body. TAG plays an important role in the storage of energy in mammals, and high expression of TAG is a biomarker of metabolic disorders and has been implicated in type 2 diabetes, obesity, and bone metastatic hepatitis.

Monoacylglycerol acyltransferase (MGAT) is an important enzyme involved in the synthesis of triglycerides after meals in humans. The catalytic process involves the acetylation of monoacylglycerol

fatty acids to diacylglycerol (DAG). The next and final step in TAG biosynthesis is the further acylation of DAGs to TAGs by second-line glycerol acyltransferases (DGATs).

Currently, there are three isozymes of MGAT inhibited in mammals. MGAT1 is mainly expressed in the stomach, kidneys, and fat cells. MGAT2 and MGAT3 are highly expressed in humans, mainly in the small intestine and liver. Systemic knockout of MGAT2 (MGAT2-/-) in mice, as well as knockout of MGAT2 in the intestine (MGAT2IKO), exhibit reduced food intake, delayed fat absorption, and increased energy expenditure. Further, these mouse models demonstrated improved insulin sensitivity and were tolerable to diet-induced obesity (DIO) and related metabolic disorders such as hypercholesterolemia and steatohepatitis. In addition, the expression of MGAT2 in non-alcoholic fatty liver disease (NAFLD) increased but decreased after gastric bypass, suggesting that this enzyme plays an important role in the development and progression of fatty liver. Recently, the authors confirmed that MGAT2 inhibitors reduce liver fibrosis and inflammation in two mouse models of nonalcoholic steatohepatitis (NASH), further supporting the concept of MGAT2 as a target for the treatment of metabolic diseases.

Lowering TAG levels is one of the strategies for the treatment of diabetes, obesity, and related metabolic disorders. This strategy is clinically validated and uses therapeutic targets that target TAG absorption pathways, such as pancreatic lipase and diacylglycerol acyltransferase (DGAT1). However, inhibitors of both enzymes have been clinically shown to be associated with intestinal adverse effects, such as diarrhea.

Since the loss of MGAT2 function in intestinal epithelial cells results in only a partial decrease in TAG levels, the loss of DGAT1 function leads to complete blockade of TAG biosynthesis. Therefore, inhibition of MGAT2 reduces the risk of mechanism-based intestinal adverse reactions associated with DGAT1 inhibitors.

BMS developed a potent and highly selective MGAT2 inhibitor, BMS-963272 (Compound 1), as the first clinical candidate for BMS, and was evaluated in Phase I clinical trials, Compound 1 can increase plasma long-chain dicarboxylic acids, show strong pharmacodynamic biomarker modulation, increase glucagon GLP-1 and PYY, and reduce subject weight.

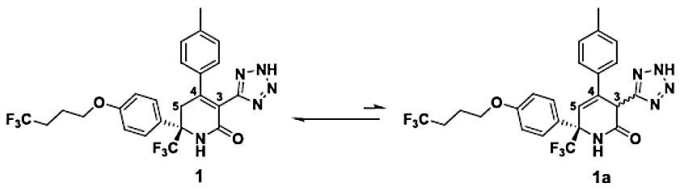

Figure 1. Isomerization of aryldihydropyridinones.

Compound 1 uses dihydropyridone as the parent nucleus, and when BMS studies the derivative structure of dihydropyridone, it is found that some lead compounds with dihydropyridone as the parent nucleus have the isomerization of C-C double bonds. Clinical-stage compound 1 contains an optimized carbon-linked tetrazolium group that shows a controlled conversion of isomers (<5%) to unstable nonconjugated isomer 1a (as shown in Fig 1), while many potent analogues of C3 substituents uncarboxylamide or cyano groups show significant isomerization to form more stable nonconjugated isomers and thus have had to abandon advancing into the clinic. In addition, it was observed that the glucuronidation rate of compound 1 was significantly different among different species. The half-life of glucuronidation was 39 minutes and 92 minutes in cynomolgus monkeys and rats, respectively, while the half-life was > 120 minutes in human, canine, and mouse liver microsomes, and high-dose

administration was required, with three doses per day showing optimal biomarker modulation to achieve weight loss.

BMS attempts to improve a range of MGAT2 inhibitors to ameliorate the problems that BMS-963272 may have with due to glucuronidation of tetrazolium and isomerization of the C-C double bond of the dihydropyrrodone parent nucleus. Compound 12 (**BMS-986172**) was identified as a second clinical candidate through a series of screenings and preclinical characterization with a favorable pharmacokinetic profile.

Table 1. C3 Heteroaryl Analogues[a,b,c,d]

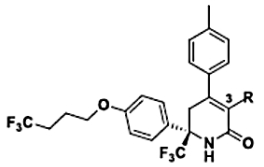

Example	R	MGAT2 LCMS IC_{50} (nM)[a]		Liver microsome metabolic stability (% remaining)[b]		UGT metabolic stability $T_{1/2}$ (min)[c]		PXR EC_{50} (μM, % of control)[d]
		h	m	h	m	h	cyno	
1		7.1 ± 0.38	18 ± 0.91	100	100	>120	39	>50, 19
2		4.5 ± 4.8	34 ± 26	100	60	>120	102	0.608, 153
3		433	>2000	93	71	>120	>120	0.845, 68
4		704	>2000	78	75	>120	>120	ND[f]
5		14 ± 15	77 ± 9.5	76	76	>120	>120	1.54, 127
6		27 ± 17	12 ± 7.1	100	96	94	>120	>29, 22

[a]Mean IC_{50} and SEM values when $n \geq 2$. [b]Metabolic stability was reported as a percent of parent compound remaining after 10 min incubation with NADPH-supplemented human (h) and mouse (m) liver microsomes. [c]*In vitro* glucuronidation assay in liver microsomes in the presence of uridine diphosphate glucuronic acid (UDPGA). [d]% of control: compound concentration from 5 nM to 100 μM and normalized by the activity of 10 μM rifampicin; the PXR transactivation assay was conducted as described by Zhu et al.[23] [f] not determined.

Structural modification and optimization, in vitro experimental verification

Firstly, the C3-substituted tetrazolium was modified, and the isomer N-substituted tetrazolium was prepared to obtain compounds 2 and 3 to study the effect of the removal of acidic substituents on biological activity. Compound 3 showed modest inhibitory activity, while isomeric compound 2 exhibited potent inhibitory activity with an IC50 of 4.5 nM**, and compound 2 showed no significant activity against other acyltransferases (**IC50>33 μM vs MGAT3, AWAT2, and DGAT1). Compared with the C-C **double bond isomerization of tetrazolium linked to the carbon chain of compound 1, the C-C double bond of compound 2, which is also a dihydropyridone parent nuclear compound, did not undergo deconjugation, and no corresponding isomers were detected in NMR. Imidazole analogue 4 has weak inhibitory activity against MGAT2, while 1,2,3-triazole analogue** 5 is a potent inhibitor with an IC50 of 14 nM. Although these compounds have low CYP inhibitory activity and hERG toxicity, these compounds have been validated by PXR transcription experiments to have high CYP-inducing activity, and there is a potential risk of drug-drug interactionsAs shown in Table 1, compounds 2 and 5 induced PXR transcriptional EC50 values of 0.608 μM and 1.54 μM for CYP3A4 when screened in HepG2 cells, respectively. In addition, Parallel Artificial Membrane Permeability Assay (PAMPA) testing found that these compounds had low permeability, possibly due to the poor water solubility of the compounds. The other is the potential tetrazolium bioelectronic isosterone tetrazolone compound6. Although similar structures have appeared in previous literature, this

substituent is rarely seen as a bioelectronic isosterome of acid substituents in pharmaceutical chemistry. In vitro experiments showed that compound 6 had potent MGAT2 inhibitory activity (IC50=27 nM) and was selective for other acetyltransferases. Compared with compound **1,** tetrazolone analogue 6 showed a lower rate of glucuronidation in cynomolgus monkeys, with a half-life of > 120 min. In vitro safety studies showed an EC50>29 μM transcriptional activity of PXR, suggesting that the risk of drug-drug interactions is very low. In addition, similar to N-chain heterocyclic substitution, no double bond isomerization of the tetrazolone 6 core backbone was found in 1H-NMR detection.

While exploring the C3-tetrazolium bioelectronic isosteres, further study the SAR of C4 and C6. Pooled SAR found that C4 phenyl-substituted and C3-cyano-substituted analogues had previously been reported. Compared to compound 1, the C4-substituted pyridine and pyrimidine analogues7 and 8 human MGAT2 inhibitory activity was reduced by 8-fold and 5-fold, respectively. (IC50=57 nM and 37 nM vs compound **1** IC50=7 nM). In addition, the **permeability of compound 7 was much lower than that of compound 1 as determined by the PAMPA experiment**. (13 vs 179 nm/sec at pH 7.4), probably due to the stronger polarity of C4 pyridine substitution. These modifications led to the introduction of a 5-membered heterocycle at the C4 position in the BMS. For C6 SAR modification, various benzene ring substitutions and side chain length modifications were tried. The introduction of an F-substituent at the 2' position of the C6 benzene ring can improve the inhibitory activity. **C6 is composed of CF3 and 2'-fluoro-4'-trifluoromethyl tert-butoxyphenyl groups are the best substituents.** Three C4 five-membered heterocyclic substitution analogues show micromolar or low-single-digit nanomol MGAT2 inhibitory activity with acceptable metabolic stability, but PAMPA permeability is lower than that of compound 1. Different rates of glucuronidation were observed for C3-tetrazolium derivatives in different species. Compounds 9 and 10 humans T1/2 > 100 min, while cynomolgus monkeys have shorter half-lives of 14 mins and 23 mins, respectively.

After determining the structure of several preferred groups at C3 and C4 positions, the BMS used the combination of preferred groups to obtain new compounds, with **CF3 and 2'-fluoro-4'-trifluoromethyl tert-butoxyphenyl as the preferred substituents for C6 substituents, and the most effective C4 heterocycles (cyclopropylmethylpyrazole, cyclopropylthiazole and ethylthiophene) were selected to form a further optimized tetrazolium isomer with tetrazolone.** Compounds 12-14 exhibit similar human MGAT2 inhibitory activity, while mouse MGAT2 inhibitory activity IC50 values range from 5 nM to 20 nM. All compounds exhibited excellent hepatic microsomal and UGT metabolic stability, and glucuronidation did not vary with species, which was consistent with previously observed results for tetrazolonones. The permeability of PAMPA can be further mentioned, but these compounds meet the efficacy criteria for entering the body. To determine the selectivity of the compounds, all known lipidyltransferases **were used to detect compounds12. The IC50 values of compound 12 for recombinant human DGAT1, DGAT2, MGAT1,** AWAT1, AWAT2, DC3, ACAT1 and ACAT2 were all above 30 μM, and the IC50 value for recombinant human MGAT3 was approximately 16 μM, indicating that compound **12 was a highly selective MGAT2-specific inhibitor.**

Table 2. C4 Heteroaryl Analogues and C3, C4 Combination SAR[a,b,c,d]

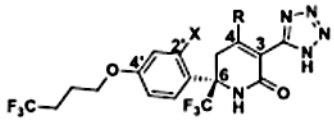

Example	R	X	MGAT2 LCMS IC_{50} (nM)[a]		Liver microsome metabolic stability (% remaining)[b]		UGT metabolic stability $T_{1/2}$ (min)[c]		PAMPA (nm/sec, pH =7.4)
			h	m	h	m	h	cyno	
7		H	57 ± 31	36 ± 3.0	100	86	ND[d]	ND	13
8		H	37 ± 3.8	7.7 ± 3.2	ND	ND	ND	ND	ND
9	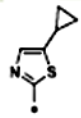	F	2.4 ± 2.0	2.3 ± 1.3	97	92	109	14	17
10	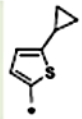	F	0.76 ± 0.42	0.73 ± 0.43	88	83	110	23	70
11	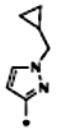	F	1.9 ± 1.8	6.5 ± 0.28	100	94	>120	76	26
12	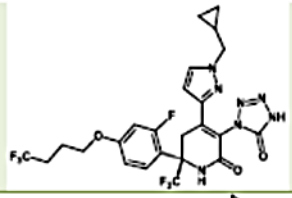		4.6 ± 2.6	20 ± 9	100	97	>120	>120	18
13	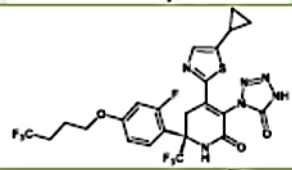		1.9 ± 1.0	6.0 ± 4.4	99	88	>120	>120	75
14	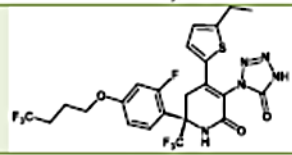		2.5 ± 2.6	4.8 ± 0.61	93	100	>120	>120	90

[a]Mean IC_{50} and SEM values when $n \geq 2$. [b]Metabolic stability was reported as percent of parent compound remaining after 10 min incubation with NADPH-supplemented human (h) and mouse (m) liver microsomes. [c]*In vitro* glucuronidation assay in liver microsomes in the presence of uridine diphosphate glucuronic acid (UDPGA). [d]Not determined.

In vivo experimental studies

The compounds were evaluated in vitro by MGAT2 enzyme experiments, other acetyltransferase selectivity, plasma protein binding activity, microsomal metabolic stability, PAMPA permeability and water solubility. Chronic weight loss in DIO mice was predicted in a model of acute 24-hour food intake in wild-type mice (the first in vivo model). In each study, animals were administered orally at a

single dose of 3 mg/kg and compound 1 at a dose of 3 mg/kg was given as a positive control. Tetrazolone-6 showed only a general effect in this experiment, reducing acute food intake by 14%. Compound 12 is potent, reducing food intake by up to 25%. Based on the results of a single dose of food intake, a 24-hour food intake dose-dependent dosing study experiment (0.01-1 mg/kg dose range, Fig 2) of compound 12 was evaluated. While positive control 1 significantly reduced 24-hour food intake, compound 12 had a greater effect on 24-hour food intake. At doses of 0.03, 0.1, 0.3 and 1.0 mg/kg, the reduction of compound 12 on food depth ranged from 21% to 34%, which was statistically significant and dose-dependent.

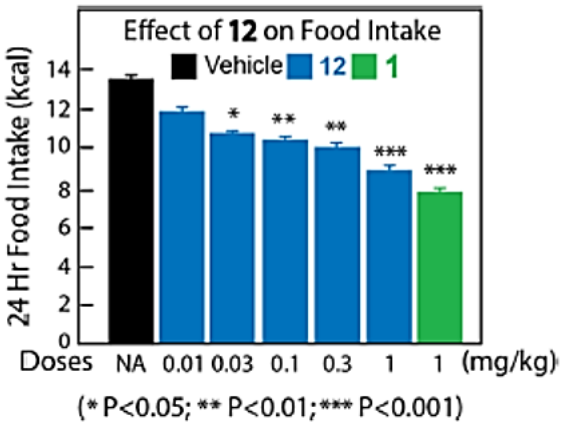

Figure 2. Effects of single-dose treatment of **12** in DIO mice on food intake in a dose–response study.

Compound 12 was evaluated for oral administration from 0.01 mg/kg to 1.0 mg/kg once daily for 21 days in a mouse model of chronic DIO. In addition to the vehicle control group (0.5% methylcellulose), compound 28e was used as the positive control group. Weight and food consumption were measured daily for 21 days. As shown in Figure 3, compound 12 had a significant reduction in body weight in the 0.1 mg/kg dose group. Body weight was reduced by 11.6%, 6.1% and 8.9% in the 0.1 mg/kg, 0.3 mg/kg and 1.0 mg/kg dose groups, respectively. Compound 12 did not exhibit a statistically significant dose-dependent effect compared to compound 1. BMS hypothesizes that reduced food intake through inhibitors by inhibiting the mechanism of action of MGAT2 is caused by GLP-1, PYY, and potentially other intestinal hormones. Elevated intestinal hormones by MGAT2 inhibitors are only the beginning of the action. Once the binding of the MGAT2 enzyme reaches its maximal level, the increase in intestinal hormone levels is not dose-dependent. Therefore, in the chronic DIO study experiment, the dose range of compound 12 was 0.01-1 mg/kg, and there was no statistical difference in weight loss. The minimum effective dose is 0.1 mg/kg.

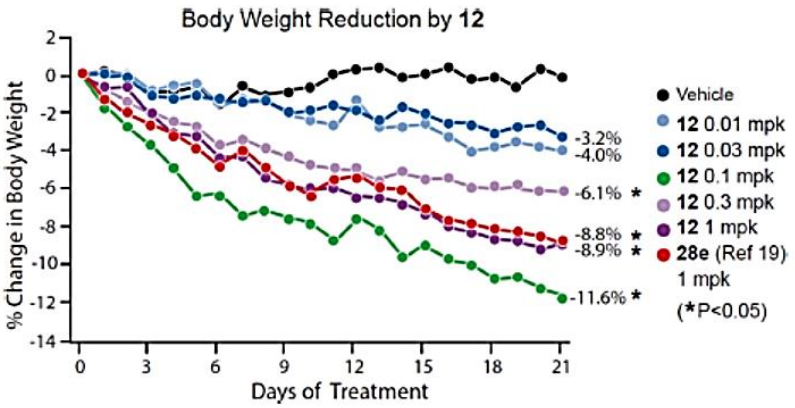

Figure 3. Effects of chronic, multiple-dose treatment of **12** on body weight in C57Bl6J-DIO mice.

In order to verify that food intake reduction and weight loss are obtained by inhibition of MGAT2 activity, experiments comparing changes in body weight and food intake at 4 days were conducted in wild-type mice and MGAT2 knockout mouse models, respectively. All mice (10 in each group) are provided with a test meal 1 week prior to dosing, followed by a daily oral administration of 3 mg/kg of compound 12 in the test for 4 days, with compound 1 as a positive control in this experiment. At the end of the study, neither compound resulted in a significant change in the body weight of MGAT2 knockout mice relative to the vehicle group. In contrast, compound 12 showed daily weight loss in all experiments in wild-type mice, and a significant reduction in the intake of compound 12 in wild-type mice, consistent with the observed changes in body weight. In contrast, no reduction in the uptake of compound 12 was observed in MGAT2 knockout mice. The lack of response to compound 12 in knockout mice also supports the mechanism-based pharmacological effects of compound 12.

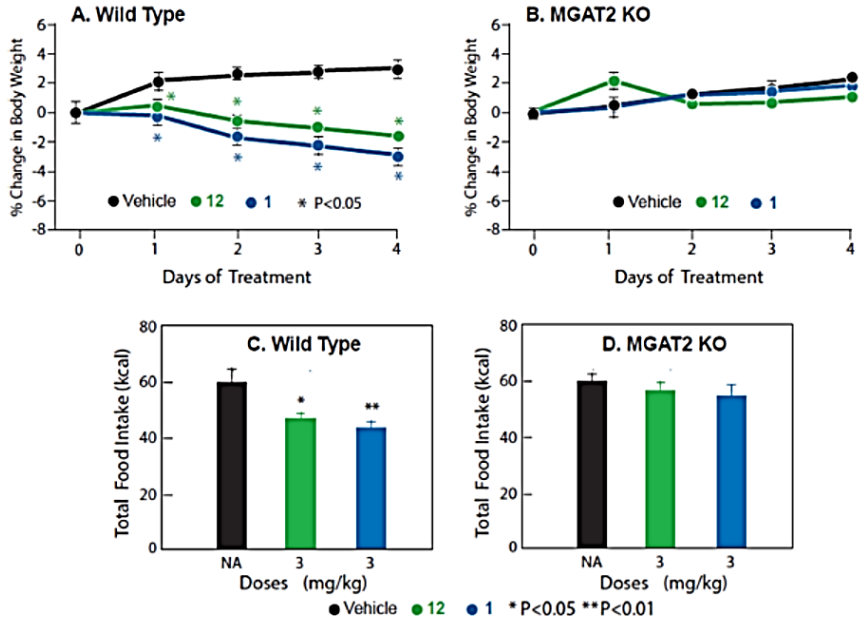

Figure 4. Effects of 3 mg/kg treatment of **12** on 4 day body weight (upper, A, B) and total food consumption (lower, C, D) in WT and MGAT2 knockout mice.

Table 3 summarizes the PK properties of compound 12 administered orally at 0.1 mg/kg in mice and rats and dogs administered orally at 3 mg/kg and intravenously administered at 1 mg/kg. Systematic clearance is lower (<30%) (relative to hepatic blood flow HBF) in mice and dogs, while higher clearance is higher in rats (30%-70%). Vss was high in rats, dogs, and mice, indicating that compound

12 had a wide tissue distribution. Among the three species, Cmax ranged from 19 nM to 1586 nM, and $AUC_{0\text{-}24\ h}$ ranged from 1.4 μM to 12 μM, with the highest exposure in dogs. The half-lives were 2.8 h, 2.5 h and 5.7 h in mice, rats and dogs, respectively. The bioavailability of oral services is moderate, ranging from 25% to 30% for different species. Compound **12 was metabolically stable after 45 min of incubation in rat, canine, monkey and human liver microsomes and hepatocytes and 24 h of hepatocytes, and more than 96% of the metabolites of all species** were parent compounds.

Table 3. PK Parameters for 12

species	mouse	rat	dog
dose (mg/kg)	1 (i.v.), 0.1 (p.o.)	1 (i.v.), 3 (p.o.)	1 (i.v.), 3 (p.o.)
vehicle[a]	H (i.v.), F (p.o.)	H (i.v.), G (p.o.)	H (i.v.), G (p.o.)
Cl (mL/min/kg)	12.5	21.0	2.37
V_{ss} (L/kg)	1.5	2.5	0.86
$T_{1/2}$ (h)	2.8	2.5	5.7
C_{max} (nM)	18.5	173	1586
i.v. AUC_{0-24} (nM·h)	2261	1355	11,984
F (%)	26	25	30

[a]Vehicle F: 0.5:0.2:99.3 v/v/v MC/Tween/water; vehicle G: 40:50:10 v/v/v PEG400/phosphate buffer/TPGS; vehicle H: 40:50:10 v/v/v PEG400/phosphate buffer/ethanol.

In high-dose PK studies, 6% of pyrazole N-dealkylated metabolites were found in rat and canine plasma. Phenyl O-dealkylation products and further glucuronidation are found in all species in the in vitro and in vivo metabolic pathways. A small amount of two glucuronic acid metabolites (<0.5%) was detected. No products produced by the human metabolic pathway were present, and no glutathione conjugates were detected.

Since the reduction in food intake and the resulting weight loss is the most important factor in predicting the clinical metabolic benefit of MGAT2 inhibitors, the dose that causes sustained weight loss in multiple dose studies of DIO mouse models is used as a human dose. Since there was no dose-dependent effect from 0.1 mg/kg/day to 1.0 mg/kg/day, BMS chose 0.3 mg/kg/day (half a logarithm higher than the minimum effective dose) as the target dose, which was able to significantly reduce food intake and reduce body weight in the DIO model.

Regarding the selection of PK parameters, plasma AUC level indicators were used as a guide. The reasons for choosing this index are: 1. MGAT2 is an intracellular enzyme in intestinal cells of the intestinal epithelium, and it is not practical to directly measure the exposure of compounds in tissues in clinical practice. By comparing oral administration and subcutaneous administration of compounds1, it was found that the level of decline in food intake matched the plasma exposure, indicating that plasma concentrations were a good surrogate for target site exposure and were able to assess exposure at the target binding site; This mechanism hypothesizes that MGAT2 inhibition in combination with fatty acids leads to the accumulation of fatty acids, which are natural ligand agonists of receptors that trigger glucagon secretion and vagus nerve responses, resulting in reduced food intake, suggesting that 24-hour exposure to the target may be unnecessary. Taking these factors into account, the AUC exposure of compound 12 in DIO mice (0.394 μM.h) at a dose of 0.3 mg/kg/day was selected to guide the human dose prediction.

According to preclinical experimental data and modeling predictions, the exposure of compound 12 was 0.143 μM.h when the human dose was 5 mg. However, in a phase I trial in healthy volunteers, 12 volunteers with a 5 mg daily dosing regimen showed a mean terminal phase half-life between 37 and 63 and a steady-state AUC (0-24) of 6.24 μM.h, which was the target AUC exposure (0.394 μM.). h) 16 times. Compound 1 had a final half-life of 1.78 hours after a single oral dose of 100 mg. Based on the whole-human PK profile, it is expected that a dose of 0.35 mg is required for compound 12 to achieve the target effective exposure, while the dose of compound 1 is 126 mg, as shown in Table 4.

Table 4. Dose Projections Based on Human PK Data from Phase 1 Studies

compound	1	12
phase 1 single dose in human	100	5
observed mean steady-state AUC_{0-24h}, μM·h	2.23	6.24
targeted efficacious AUC based on preclinical studies, μM·h	2.8	0.394
human dose projected to achieve efficacious AUC, mg	126	0.35

Overall, compound 12 (**BMS-986172**) is a novel,High selection of human MGAT2 inhibitors. Compared with compound 1, compound 12 had a different metabolite profile, with minimal glucuronide generation (T1/2>120 min) in vivo experiments in human, rat, mouse, monkey, and canine, and no detectable isomers of the C3-C4 double bond of the dihydropyridone ring. Compound 12 has no effect on MGAT2 knockout mice and reduces food intake and body weight in wild-type mice with a minimum effective dose of 0.1 mg/kg (5% weight loss). **BMS-986172 has completed a Phase I clinical trial (NCT04926051) in the U.S. and** is expected to be developed for the treatment of obesity and NASH.

Part III

1. Combined with drug design ideas, Yaodu cyberSAR excavates the structure of activity reported in the literature and patents, and uses cyberSAR to facilitate and quickly obtain the target structure of interest of R&D personnel for developing ideas, and MGAT2 inhibitors are as follows

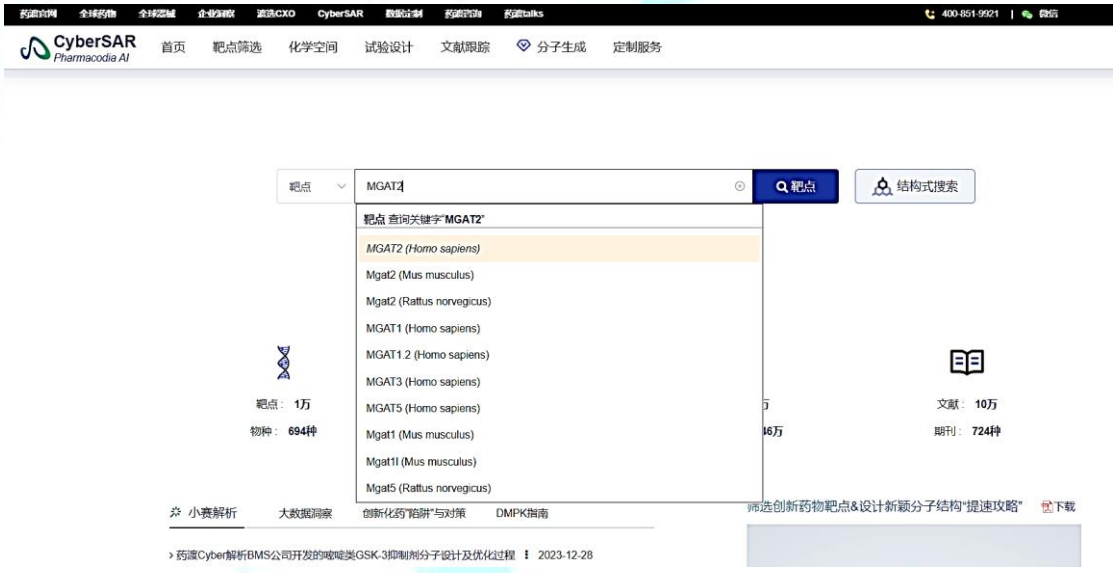

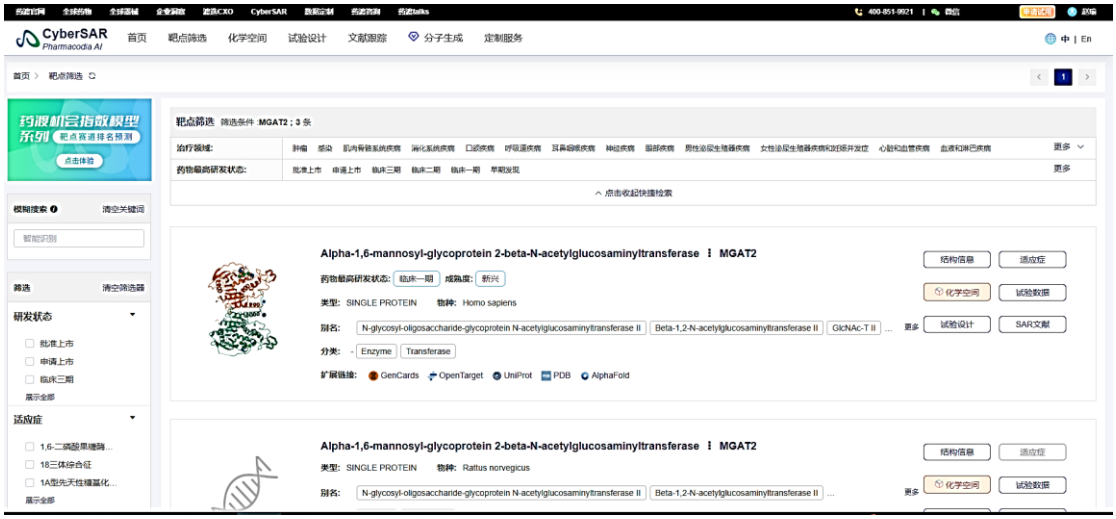

2. Select the cascade "Cluster Structure View" tab under the "Chemical Space" option tab in the target interface, and the literature and patents included in the CyberSAR platform can display the molecules with experimental test activity related to M GAT2 in the form of "parent nuclear structure clustering". Among them, the "highlighted" in green font is the active molecular structure of IC50<100 nM in the in vitro enzyme and cell activity testing experiments reported in the literature, the specific experiments, the experimental results and the experimental sources.

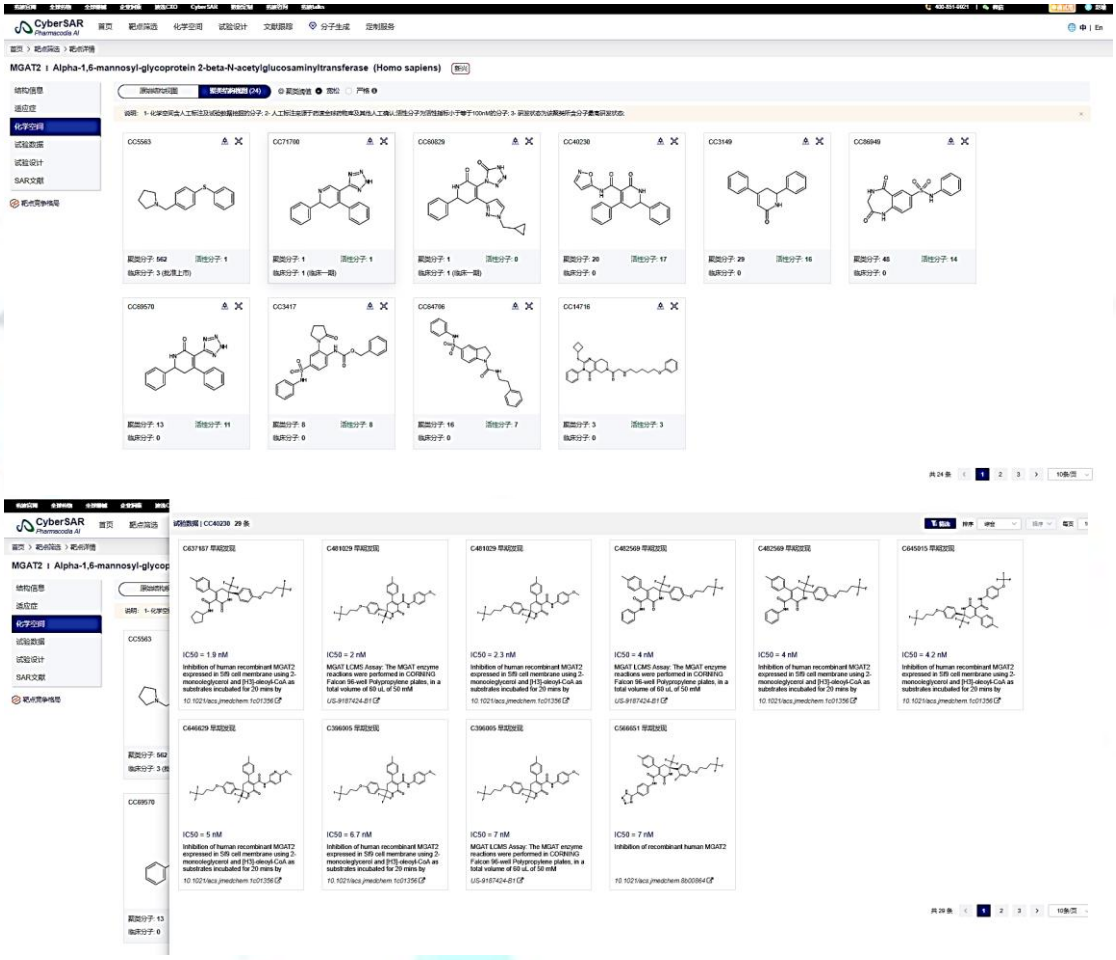

3. Select the "Chemical Space" option tab under the "Chemical Space" option tab in the target interface, and the molecules with MGAT2-related experimental test activity included in the CyberSAR platform

can be displayed in the form of "R&D stage timeline". Among them, "data mining" highlighted in green font is potential Hit.

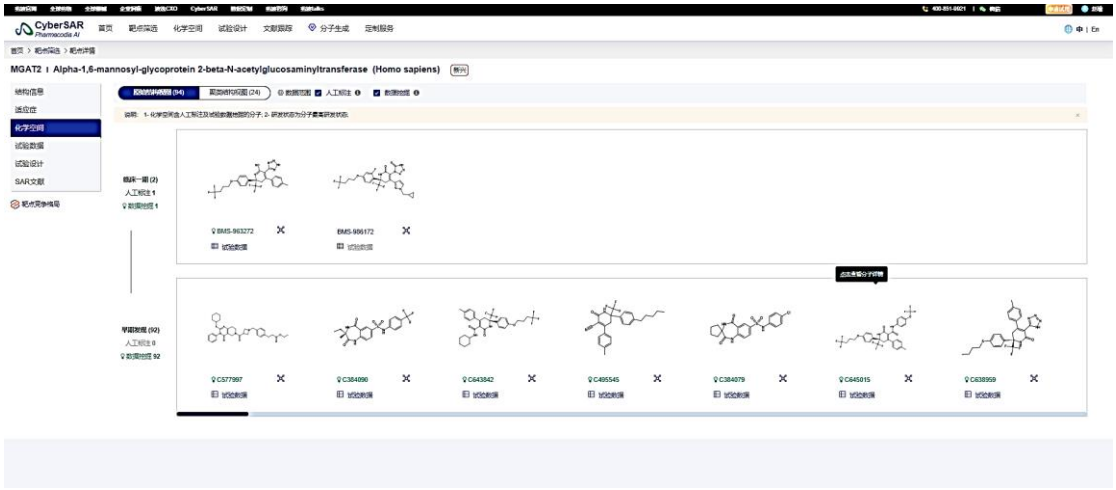

Pharmacodia GLOBAL

SaSPinjara
TRUSTED PARTNER IN EFFICIENT HEALTHCARE

CyberSAR

AI tool for innovative drug target selection and molecular design

CyberSAR
Pharmacodia AI

How can CyberSAR help you?

- Target selection
- Drug design
- Online Structure-Activity Relationship (SAR) database
- AI-Driven Exploration of Patent Chemical Space

chetans@saspinjara.com

Pharmacodiaglobal-india

http://data.pharmacodia.com/cybersar

FOR A FREE TRIAL CONTACT US ON

Sachin Marihal
+91 9538033363
sachin.marihal@saspinjara.com

Aravind. P
+91 9619076286
aravind.p@saspinjara.com

Chetan S
+91-7022031061
chetans@saspinjara.com

Why CyberSAR?

Target Selection

CyberSAR leverages advanced AI technology to intelligently analyze vast volumes of literature and patent data, automatically extracting key information with precision. It intelligently comprehends and extracts R&D data, including targets, molecular structures, and biological activities. This empowers rapid assessment of drug potential and identification of development targets."

Drug Design

Unlock precise decisions in navigating chemical space with a deep grasp of SAR data. Harnessing the DGL virtual compound library and cutting-edge algorithms, CyberSAR offers one-click molecular generation, empowering medicinal chemists in drug design. Drug-like molecules optimized with AI flows to improve efficacy, affinity, and selectivity.

Online Structure-Activity Relationship (SAR) Database

Empowered by AI, CyberSAR clusters 1 million molecules, revealing correlations in target, molecular core, structure, and activity/ADMET. Rapidly analyzing Structure-Activity Relationships (SAR), it provides a comprehensive view of millions of compounds by linking chemical structures to biological, pharmacological, and therapeutic insights.

Experimental Protocol

CyberSAR extracts in vitro/in vivo biological activity, ADME experimental protocols, which related to molecules , accelerating the design, screening and evaluation of specific experimental protocols by medicinal chemists.

Trial Customers

HENGRUI

JUMPCAN 济川药业

Luye Pharma 绿叶制药

CSPC

HANSOH PHARMA

齐鲁制药 QILU PHARMACEUTICAL

chetans@saspinjara.com